LAWRENCE
LIVERMORE
NATIONAL
LABORATORY

LLNL-PROC-814596

Scintillators and Detectors for MeV X-ray and Neutron Imaging

N. J. Cherepy

September 16, 2020

SPIE Optical Engineering + Applications
Virtual, CA, United States
August 24, 2020 through August 28, 2020

Disclaimer

Scintillators and Detectors for MeV X-ray and Neutron Imaging

N.J. Cherepy,[a] Z.M. Seeley,[a] S. Hok,[a] D. Schneberk,[a] P. Kerr,[a] S.P. O'Neal,[a] I. Oksuz,[b] M. Bisbee,[b] L.R. Cao,[b] S.A. Payne,[a] R.D. Sanner,[a] G. Stone,[a] B.F. Hobson,[a] G. Guethlein,[a] J. Hall,[a] R. Stoneking,[a] J. Mintz,[a] C. McNamee,[a] P.A. Thelin[a]

[a]Lawrence Livermore National Laboratory, Livermore, CA 94550, USA
[b]The Ohio State University, Columbus, Ohio 43210, USA.

ABSTRACT

High energy X-rays and neutrons can provide 3-D volumetric views of large objects made of multiple materials. Lens-coupled computed tomography using a scintillator imaged on a CCD camera obtains high spatial resolution, while a surface-mounted segmented scintillator on an amorphous silicon (A-Si) array can provide high throughput. For MeV X-ray CT, a new polycrystalline transparent ceramic scintillator referred to as "GLO" offers excellent stopping power and light yield for improved contrast in sizes up to a 12" field-of-view. For MeV neutron CT, we have fabricated both contiguous and segmented plates of "Hi-LY" plastic scintillator, offering light yields 3x higher than standard plastic.

Keywords: MeV neutron, MeV X-ray, Radiography, Scintillators, Transparent Ceramics, Plastic Scintillators

1. INTRODUCTION

Advances in high flux radiation sources [1-3] are being combined with new high light yield scintillator-based imaging detectors for enhanced throughput and resolution for non-destructive characterization. Lens-coupled computed tomography (CT) using a scintillator imaged on a CCD camera (Figure 1) can obtain high spatial resolution, but typically with a high dose-to-image [4]. In contrast, amorphous silicon (A-Si) arrays with a thick surface-mounted segmented scintillator can obtain images quickly, but with poorer spatial resolution. Demanding applications, such as CT of complex additively manufactured components, require both high throughput and resolution [5]. For X-ray and neutron CT, moderate light yield glass or plastic scintillators, respectively, have been used in lens-coupled imaging. The new polycrystalline transparent ceramic scintillator, "GLO," offers excellent stopping power and light yield for MeV Bremsstrahlung X-ray CT. For MeV neutron CT, a high light yield Iridium-complex-activated plastic may be employed.

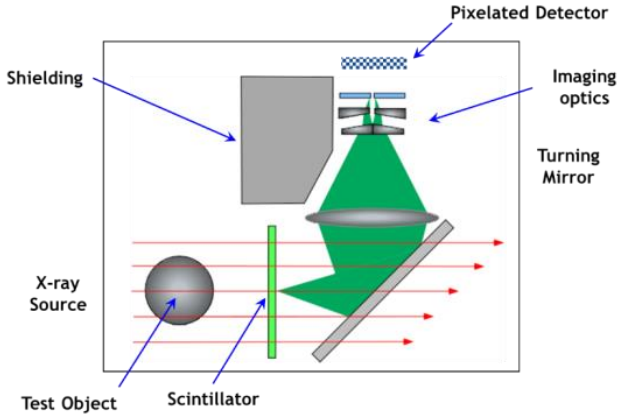

Figure 1. Typical lens-coupled imaging configuration.

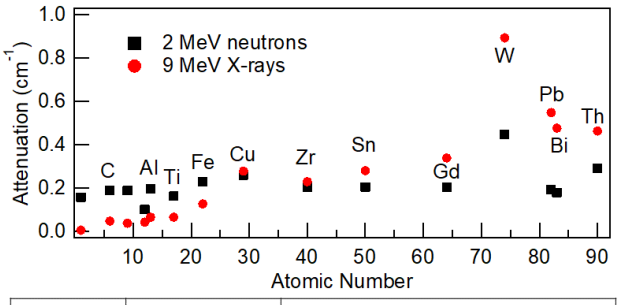

	Mean Free Path (cm)			
Radiation	HDPE	Al	W	Typical Radiation Source
2 MeV n^0	3.32	5.15	2.23	Fission neutrons from reactor or a DD source
100 keV X-rays	6.17	2.23	0.01	Typical mean energy from standard X-ray tube
3 MeV X-rays	26.30	10.46	1.27	Mean energy for 9 MeV LINAC

Figure 2. MeV neutron and X-ray stopping across the periodic table.

A moderate-light-yield scintillating glass for lens-coupled X-ray CT is known as "IQI glass" or "Tb-glass" [6]. Lu_2O_3:Eu and the analogous phosphor $(Gd,Y)_2O_3$ (HiLight^{TM}) are well-known translucent ceramics for X-ray radiography [7-9]. By partial substitution of Gd for Lu, the lattice parameter of the crystal is expanded, allowing for uniform incorporation of Eu [10], and formation of phase-pure, transparent polycrystalline $Gd_{0.3}Lu_{1.6}Eu_{0.1}O_3$, or "GLO". GLO ceramics are fabricated from nanoparticles that are hot pressed, vacuum sintered, hot isostatic pressed to full density [10,11]. GLO may be formed as a highly transparent ceramic with acceptably low optical scatter losses for use in lens-coupled imaging [12]. GLO offers excellent X-ray stopping, due to its Z_{eff} = 68 and density of 9.1 g/cm^3.

Fast neutron imaging is both benefited and complicated by the low interaction efficiency of high energy neutrons with matter. Their high penetration of even very dense materials allows MeV neutrons to see inside large, dense objects, but also makes acquisition of neutron radiographs slow, even with high flux sources, since their interactions with the detector materials are similarly poor. Figure 2 shows neutron (2 MeV) and X-ray (9 MeV) stopping across the Periodic Table, as "inverse mean free path" or stopping coefficient (cm^{-1}). Typical X-ray tubes operate in the vicinity of 100 keV, where stopping ranges from 0.3 cm^{-1} (for C) to 59 cm^{-1} (for W). The poor penetration of high-density objects thus limits the range of materials and their thicknesses that may be effectively imaged with low energy X-rays. MeV X-rays are far more penetrating; at 9 MeV, stopping ranges from 0.041 cm^{-1} (for C) to 0.892 cm^{-1} (for W). However, the poor attenuation of MeV X-rays in low-Z materials makes it difficult to acquire accurate CT of multi-material assemblies. Meanwhile, MeV neutrons provide attenuation coefficients of 0.1-0.45 cm^{-1} across the periodic table, making them better suited for imaging of combinations of high and low Z components.

A new plastic scintillator, the "Hi-LY" plastic, is based on a green-emitting Iridium complex spin-orbit-coupling fluor, such as are used in Organic Light Emitting Diodes (OLEDs). The higher light yield results from the ability of this type of fluor to efficiently scintillate when excited by both the singlet and triplet excitons created by ionizing radiation in the plastic (generated at a ratio of 25% singlets and 75% triplets, due to spin statistics). Its green emission is well-suited to readout with Silicon imaging devices. This new plastic scintillator has been tested for lens-coupled MeV neutron imaging, as well as surface-mounted segmented scintillator on A-Si arrays [13-15].

2. EQUIPMENT AND METHODS

2.1 GLO scintillator measurements

Fabrication of GLO scintillators followed established procedures [8]. X-ray attenuation radiographs were acquired using a Varian Linatron 9 MeV Bremsstrahlung source, lead collimators, 2 mm thick Tb-glass or GLO scintillator plate, turning mirror, imaging lens system (designed by Optics One) and CCD cameras (Spectral Instruments). Radiographs were flat-field corrected, background subtracted and analyzed with IMGREC software [16].

2.2 Hi-LY plastic scintillator measurements

Fabrication of Hi-LY plastics followed standard procedures [13]. Radioluminescence spectra were acquired using a Po-210 alpha source (5.4 MeV), and spectra were collected with a Princeton Instruments/Acton Spec 10 spectrograph coupled to a thermoelectrically cooled CCD camera. Scintillation pulse height spectra were acquired with radioisotope sources using a 2" Hamamatsu R6231-100 PMT. The signals from the photodetector anode were shaped with a Tennelec TC 244 spectroscopy amplifier and recorded with an Amptek MCA8000-A multi-channel analyzer.

MeV neutron radiography measurements were performed at The Ohio State University Research Reactor' (OSURR) fast neutron beam line at a flux of ~5.4 x 10^7 n/cm^{2}s @ 1.6 MeV at the collimator exit [2]. A 1-cm thick Hi-LY plastic scintillator was used, along with a front-surface mirror, and a lens-coupled thermoelectrically cooled Electron Multiplying Charge Coupled Device (EMCCD) camera. Radiographs of single element cubes were acquired separately with 1-minute exposure time and 150 EM gain. Radiographs were flat-field corrected and background subtracted.

Neutron radiography measurements were also made with a Thermo Scientific P 385 DT source (14 MeV) and a Perkin Elmer XRD 1621, 41 cm x 41 cm detector, operating at 130 kV and 70 μA.

3. RESULTS AND DISCUSSION

3.1 X-ray Imaging with 9 MeV Bremsstrahlung

The properties of Tb-glass are compared to those of the GLO scintillator in Figure 3a. Imaging throughput for 9 MeV Bremsstrahlung X-ray CT (mean energy of 3 MeV) is improved due to the higher stopping power and higher light yield of the GLO by about 7x. Our previous efforts confirm that the improvement is of this order or better, depending on shielding and experimental configuration [3,12]. Figure 3b shows a transparent ceramic GLO scintillator plate, 12" x 12" x 0.1" thick. The GLO imaging plates outperform scintillator glass for MeV radiography, due to higher light yield (55,000 Ph/MeV) and better stopping, while providing spatial resolution of >8 lp/mm for MeV X-rays.

Scintillator	ρ (g/cm³)	α_γ (cm⁻¹) @ 3 MeV	Light yield Ph/MeV	FOM	lp/mm @ 3 MeV
Tb-glass	3.8	0.14	20,000	1.0	7.3
GLO	9.1	0.36	55,000	7.1	8.5

Figure 3a. Comparison between Tb-glass and GLO scintillator.

Figure 3b. 12" transparent ceramic GLO plate.

For a scintillator to prove useful for high flux and long duration CT applications, radiation hardness and resistance to radiation darkening is important. The well-known X-ray ceramic, HiLight™, $(Y,Gd)_2O_3$:Eu, has been reported to exhibit slight radiation darkening that saturates at a low dose, and this effect does not degrade the performance of Hilight in X-ray imaging [8,9]. To explore the radiation-induced darkening of GLO and Tb-glass, a study was conducted exposing 2.2 mm thick pieces of each scintillator to a Co-60 source, and periodically removing the scintillators from the irradiator to acquire optical absorption spectra, as shown in Figures 4a-4c. Very mild reduction in optical transmission at the scintillation wavelength for both scintillators was measured, likely due to trapped electrons forming "color centers." The reduction in transmission achieves steady-state (saturates) at <1.5%/mm, at a cumulative dose of 130 kR (GLO) and 2 MR (Tb-glass), after which no further darkening occurs for either scintillator for the duration of testing up to 7 MR. Radiation darkening in GLO disappears at room temperature when held in the dark after about 14 days, or within a few minutes in room lights, while the Tb-glass must be thermally annealed to remove darkening.

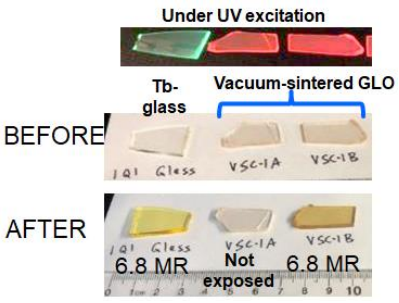

Figure 4a. Three scintillators: **(top row)** Under UV excitation, **(middle row)** In room lights, and **(bottom row)** After 6.8 MR irradiation with a Co-60 source.

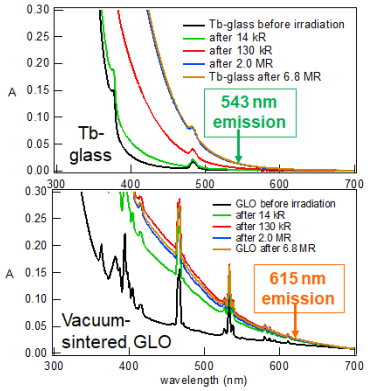

Figure 4b. Optical absorption spectra of: **(top)** Tb-glass, each trace acquired after various cumulative doses, and **(bottom)** GLO at the same doses.

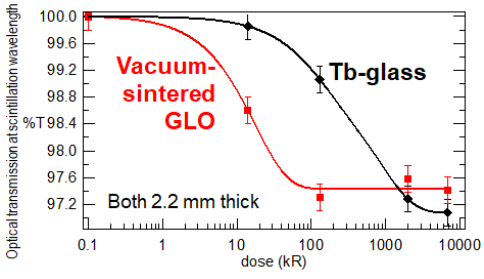

Figure 4c. At the scintillation emission peaks for Tb-glass (543 nm) and GLO (615 nm) the absorption spectra from Figure 4b are analyzed and the decrease in optical transmission tracked, saturating at ~97%.

Figure 5a shows a multi-material phantom constructed from high-density components. Figure 5b shows the attenuation radiograph, flat-field-corrected and background subtracted, acquired with Tb-glass, an average of 8 frames of exposure time 12 s each. For the camera read time of 3s/frame, the total acquisition time was 120 s. Figure 5c shows a comparable radiograph acquired with GLO, but this time with 8 frames of exposure time 0.75 s each, for a total acquisition time of 30 s, mainly limited by the camera read time. Compared to Tb-glass, the GLO scintillator provides a significant contrast-to-noise improvement for faster imaging throughput, as well as slightly improved spatial resolution.

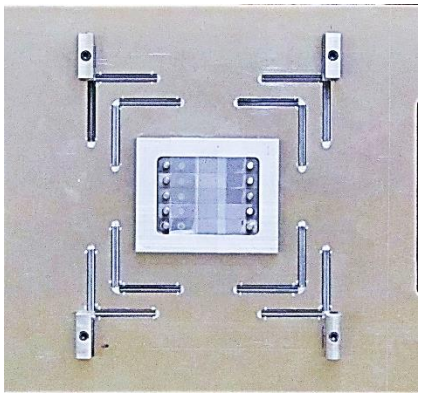

Figure 5a. Photograph of multi-material phantom used to acquire attenuation radiographs with 9 MeV Bremsstrahlung, (Figures 5b and 5c).

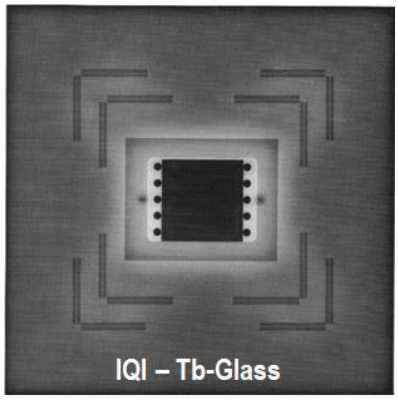

Figure 5b. Attenuation radiograph, acquired with the Tb-glass scintillator. Image acquisition time was 96 s, read time of 24 s (120 s total).

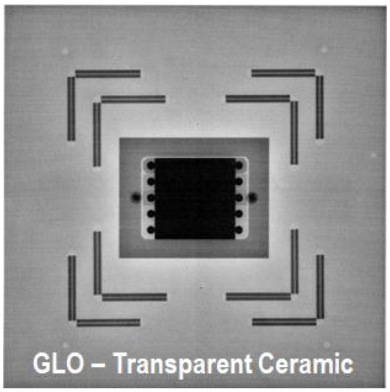

Figure 5c. Attenuation radiograph, acquired with the GLO scintillator. Image acquisition time was 6 s, read time of 24 s (30 s total).

3.2 Fast Neutron Imaging

A high light yield plastic scintillator can enhance performance for both lens-coupled imaging and A-Si panels with a surface-mounted segmented scintillator plate. Lens-coupled radiography with MeV neutrons has typically employed standard plastic scintillator, limited to about 10,000 Ph/MeV light yield. The new Hi-LY plastic offers all the advantages of standard plastic, such as transparency and ease of manufacture in large sheets, with an improved light yield. MeV neutron imaging can also be performed with an A-Si array with a surface-mounted ZnS:Cu phosphor/polypropylene screen. Figure 6a compares the alpha-excited light yield of the ZnS:Cu/PP screen with several transparent plastics, identifying Iridium complex 1, which provides an integrated light yield comparable to that of the ZnS:Cu (Figure 6b).

UV excitation				
	backlit			
	ZnS:Cu in PP	Ir-Complex 1	Ir- Complex 2	Singlet fluor
Rel. α LY (backside irradiated)	1	1	0.78	0.29
Spatial resolution	~2 mm on amorphous Si panel	Lens-coupled ~100 um		

Figure 6a. The standard ZnS:Cu/polypropylene scintillator screen is compared with several transparent plastic scintillators. Iridium complex #1 is about 3x brighter than a blue-green emitting singlet fluor plastic scintillator.

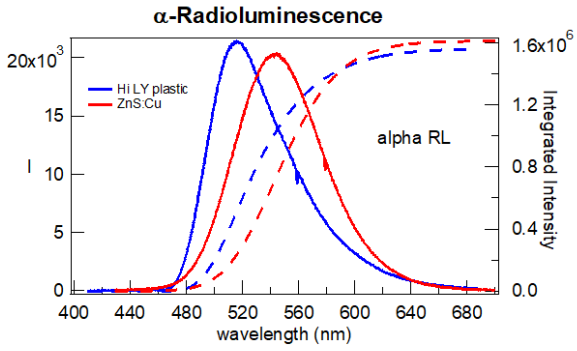

Figure 6b. The alpha radioluminescence light yields of the Hi-LY plastic **(blue)** and the ZnS:Cu/PP scintillators **(red)** are comparable. However, in contrast to the opaque ZnS:Cu/PP, the transparent plastic may be made thick for higher efficiency.

Fabrication of large transparent plates for large field-of-view lens-coupled imagers is in progress, as well as voxelated or segmented scintillator plates for use on an A-Si array (Figure 7a). High-performance segmented scintillator blocks require: excellent polish on all sides of the segments, high reflectivity reflector that blocks light from being transmitted between segments, and close-packing to avoid dead-space. Figure 7b shows that the pulse-height spectra acquired with Cs-137 of the segmented block and a single voxel. The segmented block actually exhibits a slightly higher light yield (channel number of the Compton Edge), due to use of more reflector material in the packed block.

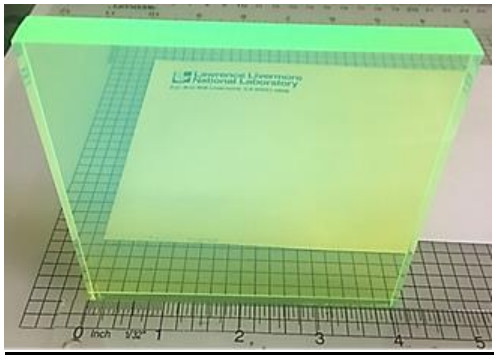

Figure 7a. (left) A 4" x 4" plate of the Hi-LY plastic scintillator, under UV excitation. **(top right)** A segmented Hi LY plastic for use with an amorphous Si array, in room lights. **(bottom right)** Same segmented plastic under UV excitation.

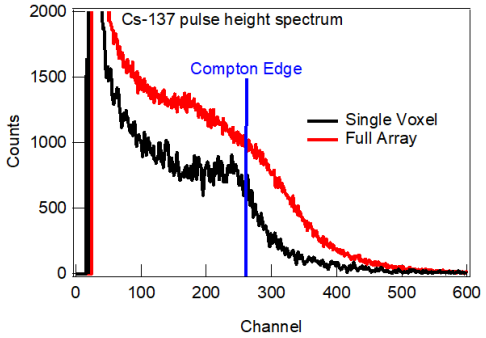

Figure 7b. Performance of the segmented scintillator is comparable in light yield to that of a single voxel from the array, indicating excellent light collection in this geometry.

A Hi-LY plastic plate similar to the one shown in Figure 7a was used in the lens-coupled system at Ohio State University [2]. As a means of evaluating spatial resolution and validating neutron attenuation coefficients, six 1" cubes of pure elements were imaged: Graphite, Aluminum, Titanium, Iron, Copper and Tungsten were set at a 1 mm standoff from the scintillator and imaged (Figure 8). These results indicate that spatial resolution of 60-100 um can be obtained in this configuration, depending on the materials being imaged. Degradation in resolution and accuracy of the measured transmission is influenced by higher "in-scatter" from the object into the scintillator for the lower density materials.

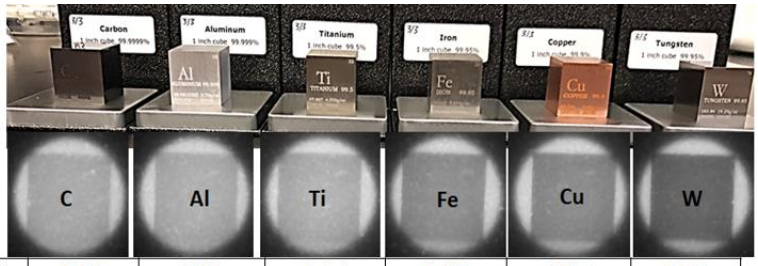

	C	Al	Ti	Fe	Cu	W
T (Meas)	0.86	0.85	0.84	0.70	0.67	0.53
Res. (um)	91	99	89	78	81	57

Figure 8. (top) Six 1" cubes of elements spanning much of the Periodic Table were measured at the Ohio State University Research reactor. **(middle)** Transmission radiographs of each cube. **(bottom)** Measured fractional transmission values and spatial resolution.

Figure 9 shows experiments performed with a D-T neutron source and an amorphous Silicon panel with surface-mounted scintillators. A segmented Hi-LY block, as shown in Figure 7a, was fabricated with 5 mmx 5 mm cross section voxels, 25.4 mm thick. The Hi-LY block was surface mounted side-by-side with a ZnS:Cu/polypropylene screen. The Hi-LY scintillator was found to provide 4.6X brighter signal, compared to the ZnS screen, using a highly attenuating Tungsten block to compare with the open-field brightness.

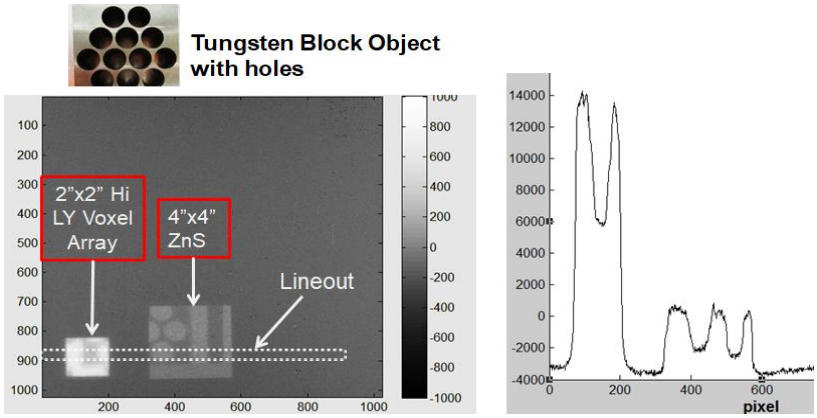

Figure 9. (left top) Tungsten block with holes, used for measurement. **(left bottom)** Image from the A-Si panel with two different surface-mounted scintillators, the Hi-LY plastic segmented block and a piece of ZnS:Cu/polypropylene. **(right)** The lineout shown reveals the Hi-LY plastic is about 4.6X brighter than the ZnS screen.

4. CONCLUSIONS

Transparent ceramic GLO can improve throughput for MeV radiography. It has been scaled up to 12" optically transparent plates that offer spatial resolution slightly better than the standard glass scintillator, while the combined light yield and stopping power improvement results in >7x higher effective light yield. High energy neutron radiography performed with lens-coupled imaging or A-Si arrays can employ the new Hi-LY plastic to acquire data significantly faster than with standard plastic scintillator, for the same scintillator geometry.

ACKNOWLEDGEMENTS

Thanks to the many collaborators on these efforts, including staff at Pantex, Los Alamos, Y-12, Varian, VJ Technologies, Radiabeam, Eljen, CoorsTek, TA&T, American Isostatic Presses, Bodycote, and Nanocerox. This work was supported by the US DOE, Office of NNSA A&L Program, MTP, NA-22 and LLNL-LDRD 20-SI-001. It was performed under the auspices of the U.S. Department of Energy by Lawrence Livermore National Laboratory under Contract DE-AC52-07NA27344. LLNL-PROC-814596

REFERENCES

1. J. H. Vainionpaa, et al, "High yield neutron generators using the DD reaction," AIP Conf. Proc., 1525, 118 (2013).
2. I. Oksuz, et al, "Characterization of a reactor-based fast neutron beam facility for fast neutron imaging." Hard X-Ray, Gamma-Ray, and Neutron Detector Physics XXII 11494, 114940T (2020).
3. D. Tisseur, et al., "Performance evaluation of several well-known and new scintillators for MeV X-ray imaging," 2018 IEEE (NSS/MIC), Sydney, Australia, 1-3 (2018).
4. J.E. Trebes, et al, Proc. SPIE. 3149, "Developments in X-Ray Tomography," 173, 0277-786X (1997).
5. http://old.digitaleng.news/de/combine-ct-scanning-additive-manufacturing/
6. P. Pavan, et al, "Radiation damage and annealing of scintillating glasses," Nucl. Instr. Meth. Phys. Res. B, 61, 487-490 (1991).
7. A. Lempicki, et al, "A new lutetia-based ceramic scintillator for X-ray imaging," Nucl. Instr. Meth. Phys. Res. A, 488, 579 (2002).
8. W. Köstler, et al, "Effect of Pr-Codoping on the X-ray Induced Afterglow of $(Y,Gd)_2O_3$:Eu," J. Phys. Chem. Solids, 56, 7, 907-913 (1995).
9. S.J. Duclos, et al, "Development of the HiLight™ scintillator for computed tomography medical imaging," Nucl. Instr. Meth. Phys. Res. A,505, 1–2, 68-71 (2003).
10. Z. Seeley, et al, "Two-step sintering of $Gd_{0.3}Lu_{1.6}Eu_{0.1}O_3$ transparent ceramic scintillator," Opt. Mater. Express 3 (7), 908-912 (2013).
11. Z. Seeley, et al, "Phase stabilization in transparent Lu_2O_3: Eu ceramics by lattice expansion," Opt. Mater., 35, 74-78 (2012).
12. N.J. Cherepy, et al, "Transparent ceramic scintillators for gamma spectroscopy and MeV imaging," Proc. SPIE 9593, Hard X-Ray, Gamma-Ray, and Neutron Detector Physics XVII, 95930P (2015).

13. Chuirazzi, et al, “Evaluation of Polyvinyl Toluene Scintillators for Fast Neutron Imaging” J. Radioan. Nucl. Chem. 318, 543-551 (2018).
14. I. Oksuz, et al, “Characterization of Polyvinyl Toluene (PVT) scintillators for fast neutron imaging,” SPIE Hard X-Ray, Gamma-Ray, and Neutron Detector Physics XX 10762, 107620D (2018).
15. N.J. Cherepy, et al, “New Plastic Scintillators for Gamma Spectroscopy, Neutron Detection and Imaging,” IEEE Nuc. Sci. Symp. Conf. Rec. 2017, (2018).
16. R. Brancaccio, et al., “Real-Time Reconstruction for 3-D CT Applied to Large Objects of Cultural Heritage,” IEEE Trans. Nucl. Sci., 58, 4, 1864-1871 (2011).